Gratings with an aperiodic basis: single-mode emission in multi-wavelength lasers

2011 New J. Phys. 13 113023

(http://iopscience.iop.org/1367-2630/13/11/113023)

New Journal of Physics
The open-access journal for physics

Gratings with an aperiodic basis: single-mode emission in multi-wavelength lasers

R Blanchard[1], S Menzel[1], C Pflügl[1,2], L Diehl[1,2], C Wang[3], Y Huang[4], J-H Ryou[4], R D Dupuis[4], L Dal Negro[5] and F Capasso[1,6]

[1] School of Engineering and Applied Sciences, Harvard University, Cambridge, MA 02138, USA
[2] Eos Photonics Inc., 30 Spinelli Place, Cambridge, MA 02138, USA
[3] MIT Lincoln Laboratory, 244 Wood Street, Lexington, MA 02420, USA
[4] Center for Compound Semiconductors and School of Electrical and Computer Engineering, Georgia Institute of Technology, Atlanta, GA 30332-0250, USA
[5] Department of Electrical and Computer Engineering, Boston University, Boston, MA 20036, USA
E-mail: capasso@seas.harvard.edu

New Journal of Physics **13** (2011) 113023 (13pp)
Received 13 September 2011
Published 17 November 2011
Online at http://www.njp.org/
doi:10.1088/1367-2630/13/11/113023

Abstract. We propose a new class of gratings having multiple spatial frequencies. Their design relies on the use of small aperiodic grating sequences as unit cells whose repetition forms a superlattice. The superlattice provides well-defined Fourier components, while the choice of the unit cell structure enables the selection, modulation or suppression of certain Fourier components. Using these gratings to provide distributed feedback in mid-infrared quantum cascade lasers, we demonstrate simultaneous lasing on multiple well-defined and isolated longitudinal modes, each one having a sidemode suppression ratio of about 20 dB.

[6] Author to whom any correspondence should be addressed.

Contents

1. Introduction

Coverage of the mid-infrared region of the electromagnetic spectrum is of great importance for scientific and technological applications, ranging from free-space communication to chemical spectroscopy and aircraft countermeasures. With the recent improvements in output power up to the watt level in continuous-wave [1], as well as their intrinsic flexibility of design, quantum cascade lasers (QCLs) now appear as an ideal mid-infrared light source.

It was realized early in the development of QCLs [2] that these lasers have several particularities that make them attractive for broadband or multi-band operation. As they rely on intersubband (IS) transitions, their gain spectrum is not set by the bandgap of the materials used, but can be selected by bandstructure engineering. Furthermore, as the IS transitions give rise to Lorentzian lineshapes, the energy distribution of the light that is emitted or absorbed is peaked at the energy difference between the subbands, which makes the heterostructure mostly transparent to light with frequencies outside the gain spectrum. Many different active regions can thus be stacked on top of each other in the same waveguide, aided by the fact that electrons keep cascading from one active region to the other as they remain in the conduction band while traversing the device. These characteristics of QCLs can be used to generate very wide composite gain spectra and achieve simultaneous broadband lasing [2]. Broad-gain QCLs can also be realized using a homogeneous active region composed of the repetition of a unique cascade design, as in the so-called bound-to-continuum QCLs [3], or as impressively demonstrated with more recent developments in bandstructure engineering [4, 5].

While the main focus in recent years has been on developing tunable QCLs, with a single lasing frequency scanned over the gain spectrum, e.g. by means of an external grating (EC-QCLs) [6] or an array of single-mode lasers [7], some applications, especially in the field of spectroscopy and ranging, would benefit from simultaneous lasing at several well-defined wavelengths. In particular, a multi-wavelength QCL could be used to implement multi-component gas analysis and differential spectroscopic techniques such as differential absorption LIDAR (light detection and ranging), a very sensitive technique for trace gas sensing [8]. In addition, multi-wavelength QCLs could be useful as multi-channel sources in wavelength-division multiplexing (WDM) free-space optical communication, as a high-brightness broadband source for Fourier transform infrared spectrometers and optical coherence tomography systems [9], or for room-temperature difference-frequency generation of terahertz light [10].

We demonstrate here such a multi-wavelength QCL operating on a few well-defined wavelengths, each of these being ‘single-mode’ in the sense that their sidebands are strongly

suppressed. In order to achieve this result, we devise a new class of gratings having multiple interleaved spatial frequencies.

2. Multi-wavelength lasers

A common method of obtaining single-mode emission of a semiconductor laser is to use a grating defined directly in the laser waveguide to provide distributed feedback (DFB) [11]. In such DFB lasers, the periodic modulation of the refractive index introduced by the grating opens a gap at the Brillouin zone boundary in the waveguide dispersion relation. At the edges of the gap, the group velocity goes toward zero, which corresponds to a very high density of optical states. The laser will thus likely operate on one of these two gain-favored band-edge modes. Note that in the case when the two modes experience approximately the same amount of gain and loss, true single-mode operation may be prevented. A common solution is then to introduce a $\lambda/4$ spacer in the middle of the grating. The laser will now operate at the wavelength corresponding to the defect state that is created within the photonic bandgap. It corresponds to fields localized at the defect and exponentially decaying on both sides into what now amounts to two sets of Bragg reflectors. This simple picture is valid in the case of *index*-coupled DFB lasers, i.e. when the real part of the refractive index is periodically modulated. *Gain*-coupled DFB lasers have also been demonstrated and they present a different behavior, with in particular the absence of a bandgap in frequency [11]. In this paper, we focus on *index*-coupled DFB lasers.

An early demonstration of a two-color QCL used two DFB gratings defined side by side on top of a laser waveguide [12]. This simple multi-section design is, however, impractical for lasing on a larger number of wavelengths. More generally, multi-wavelength lasing can be achieved by using a grating whose Fourier spectrum contains several discrete peaks, each corresponding to the opening of a gap in the waveguide dispersion relation. An example of such a grating is given by a sampled grating, developed initially as a means to obtain a wide tuning range in distributed Bragg reflector (DBR) semiconductor lasers [13]. It can be described as a standard first-order periodic grating with period $\delta \simeq \lambda/2$ (a Bragg grating) in which a number of grating elements are removed periodically to create a 'superlattice' with period $\Delta > \delta$. In other words, the structure of the grating is that of a standard periodic grating multiplied by a sampling square function imposing a superperiodicity. The corresponding Fourier spectrum is obtained as the convolution of the Fourier transform of the grating and that of the sampling function and features a set of narrow peaks.

We prefer an alternative description of sampled gratings as represented in figure 1, where the structure is seen as the convolution of a short grating with a long lattice of delta functions. The Fourier transform of such a structure is thus obtained by multiplying the Fourier transform of the finite-length lattice, an infinite array of narrow sinc-shaped peaks, with the Fourier transform of the short grating that forms a broad envelope. This is reminiscent of the picture crystallographers use when describing crystal lattices with a basis [14]. Indeed, some crystals can be described as a Bravais lattice where each unit cell is itself composed of several atoms. When studying x-ray diffraction patterns of these crystals, considering only the Bravais lattice is not sufficient and one needs to add a structure factor to include the interference of scattered fields coming from different atoms within a unit cell. This structure factor is a Fourier transform of the unit cell. The total scattering amplitude can be calculated by multiplying the Bravais lattice scattering amplitude with the structure factor.

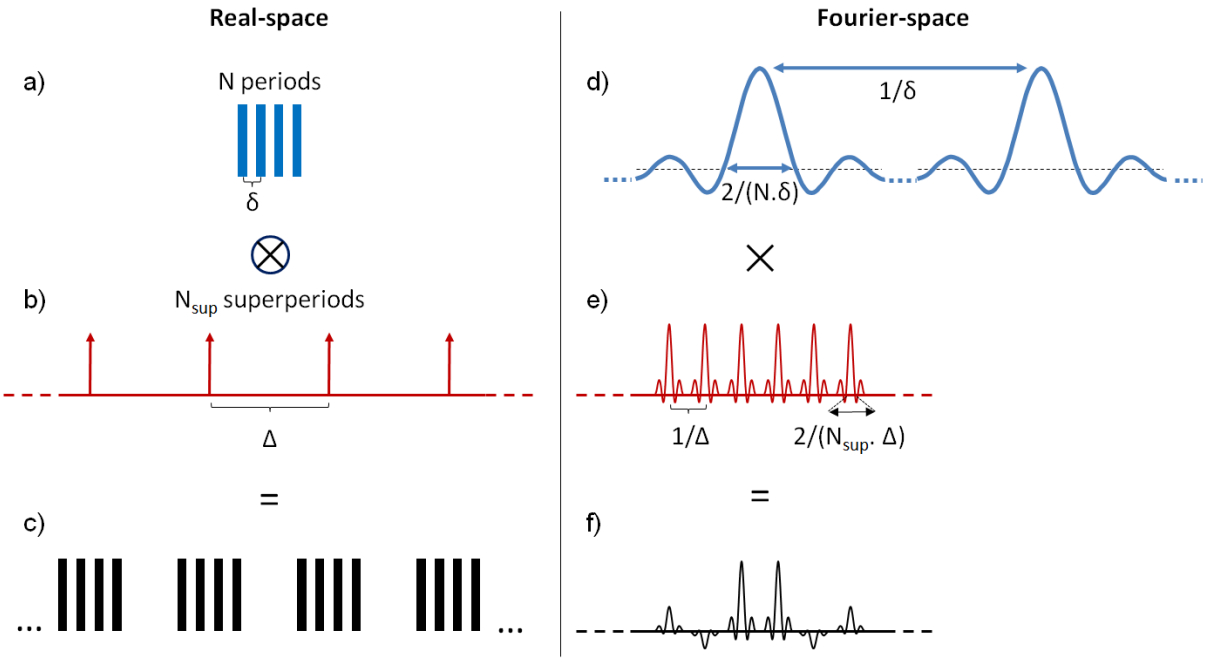

Figure 1. Schematic diagram of a sampled grating in real space and Fourier space. The sampled grating (c) is formed as the convolution of a short N-element section of a δ-periodic grating (a) and an N_{sup}-element Δ-periodic comb of delta functions (b). The thick vertical bars represent the spatial refractive index profile (succession of low- and high-index layers) that constitutes the physical grating. We assume that $N \cdot \delta < \Delta$ and $N_{\text{sup}} \gg 1$. Not represented on the schematic is the fact that the short N-element section itself can be seen as the multiplication of a boxcar function of width $N \cdot \delta$ by an infinite δ-periodic grating. The Fourier transform of the short N-element section is thus the convolution of the Fourier transform of a boxcar function, i.e. a sinc-function of width $2/(N \cdot \delta)$, with the Fourier transform of an infinite δ-periodic grating. It is thus an infinite series of sinc-functions spaced by $1/\delta$, with a large-scale amplitude modulation (not represented on the schematic diagram), corresponding to the Fourier transform of the δ-periodic grating unit cell (d). We are interested only in the first sinc-shaped peak, corresponding to the first order of the grating. The Fourier transform of the full sampled grating (f) is obtained as the multiplication of that sinc-function by the Fourier transform of an N_{sup}-element Δ-periodic comb of delta functions (e), i.e. an infinite $1/\Delta$-periodic comb of sinc-functions of width $2/(N_{\text{sup}} \cdot \Delta)$.

Our understanding of these sampled gratings as being the convolution of a periodic array with a short first-order grating section opens interesting perspectives for the design of more general multi-wavelength gratings. Let us consider a grating composed of the periodic repetition of a small aperiodic grating element, i.e. whose layers are arranged following an arbitrary sequence (figure 2(a)). Its real-space structure is formed as the convolution of the short aperiodic sequence with a finite comb of delta functions. As described above, the Fourier transform is obtained as the multiplication of the Fourier transform of the comb of delta functions by the envelope function formed by the Fourier transform of the short grating sequence (figure 2(b)).

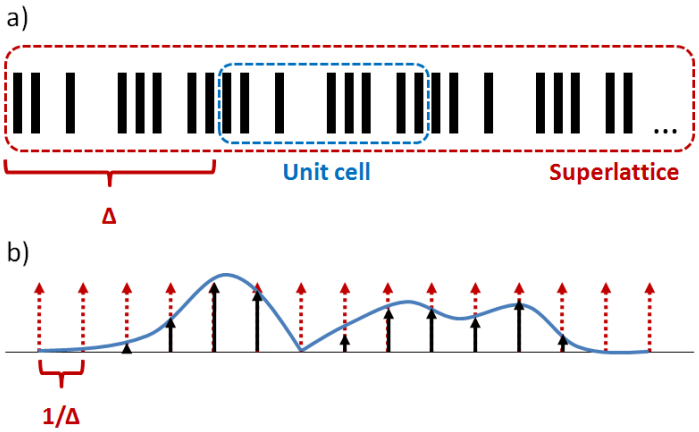

Figure 2. Schematic diagram of a grating with an aperiodic basis (GAB). (a) Real-space structure, with a unit cell of length Δ repeated periodically to form a superlattice. The thick vertical bars represent the spatial refractive index profile that constitutes the physical grating. (b) Fourier space. The Fourier transform of the grating (black) is obtained by multiplying the Fourier transform of the superlattice (red) with the Fourier transform of the unit cell (blue). For simplicity, narrow sinc-functions are represented by arrows in the Fourier spectra.

By proper design of this short element, we can shape an envelope to select, modulate or suppress specific teeth of the underlying comb of frequencies. If such a grating is integrated into a laser waveguide, we expect lasing to occur at the edges of the bandgaps corresponding to the different Fourier transform peaks. We emphasize that these peaks are due to the superperiodicity of the grating, and their amplitude is modulated by the interference between the different scattering paths within each unit cell. We will refer to these gratings as gratings with an aperiodic basis (GABs).

GABs are a generalization of sampled gratings where instead of a short periodic array we use an aperiodic array as the unit cell. Another particular implementation of this general concept is given by periodically chirped or superstructure gratings [15]. These gratings rely on a periodic modulation of the grating periodicity or of the grating phase. By opening the range of possible unit cells to aperiodic sequences, GABs enable us to use an entire new range of properties in the gratings design in particular the properties of deterministic aperiodic sequences rooted in number theory [16].

While the gratings discussed here are based on a comb of modes stemming from a superperiodicity, a more direct approach exists to obtain a small number of discrete peaks in the Fourier spectrum of a grating. It consists of superimposing sine gratings with different periodicities. The Fourier transform being a linear operation, the Fourier spectrum of the resulting grating will be the sum of the different Fourier spectra of the underlying gratings. As an analogue superposition of sine gratings presents many fabrication challenges, the concept was best implemented after binary digitization of the multi-component grating, forming a sequence of low- and high-refractive-index layers (hence the term *binary*) [17]. The digitization represents only an approximation of the analogue grating and introduces higher harmonics. A fine sampling frequency is necessary to obtain good performances. These binary superimposed gratings (BSG) offer the advantage of having built-in degrees of freedom to set the individual positions and amplitudes of the reflection peaks.

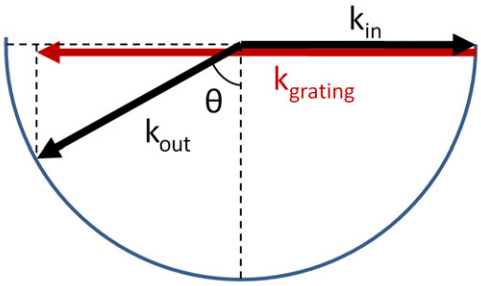

Figure 3. Schematic diagram of grating scattering. Light impinges on the grating with wavevector k_{in}. The grating provides the momentum k_{grating}. The outgoing wavevector k_{out} must lie on the blue circle representing conservation of energy. Conservation of in-plane momentum then sets the outgoing direction.

Multi-wavelength operation has also been reported by Mahler *et al* [18] using quasi-periodic DFB lasers based on a Fibonacci sequence. The particularity of this sequence lies in its pure-point measure with discrete Fourier peaks at irrational ratios [16, 19]. As discussed before, each peak corresponds to the opening of a bandgap at the edges of which a lasing mode can be selected. However, this design presents only limited flexibility in terms of peak position and amplitude. In the context of GABs, one could imagine using a Fibonacci sequence within the unit cell to obtain an envelope selecting several spectral regions.

We have so far presented different strategies to design a grating having several well-defined spatial frequencies. For the rest of this paper, we will focus on GABs because we consider that the great flexibility offered by the design of the unit cell offers interesting perspectives, both from a technological and a fundamental point of view. While it is true that the Fourier components are weaker for GABs than for BSGs, high coupling coefficients are not always desirable for QCLs. It is usually assumed that the optimal coupling coefficient κ of a DFB grating is such that $\kappa L = 1$, where L is the length of the laser cavity [11]. This ensures a good balance between the outcoupling efficiency and the overlap between the optical mode and the gain medium. Since typical lengths L for QCLs are of the order of a few millimeters, a low coupling coefficient is often preferred. In the limit of lasing on several narrowly spaced wavelengths, a low coupling coefficient would also be necessary as it results in spectrally narrow bandgaps and thus avoids their overlap. GAB lasers could also present advantages in terms of fabrication yields for applications requiring precise wavelengths of operation. Since their unit cell may feature long uniform sequences of successive similar index layers for which overexposure has practically no impact, the optical length of the unit cell (i.e. the superperiod) should be robust to such fabrication errors and thus the relative error on the lasing wavelength is likely to be lower than for DFB or BSG lasers.

Scattering losses might impact device performance for multi-wavelength grating lasers. Until now in our analysis of the gratings, we considered a purely one-dimensional (1D) problem. However, as represented in figure 3, when $k_{\text{grating}} < 2k_{\text{in}}$, there is a scattering path for an outgoing wave whose direction is not parallel to the laser waveguide. If the angle θ formed between the normal to the waveguide layers and the outgoing wavevector is smaller than the total internal reflection angle at the waveguide walls, light will leak out of the laser waveguide and will be absorbed in the laser substrate. Because the gratings we study here are based on a comb of modes, this seems to be a particularly strong concern. Indeed, the gratings have many Fourier

components such that $k_{\text{grating}} < 2k_{\text{in}}$, each corresponding to an additional scattering path. From Parseval's theorem applied to a numerical sequence with a flat Fourier spectrum over a compact bandwidth, the amplitude of the peaks in the Fourier spectrum can be considered inversely proportional to the number of peaks. The sum of the GABs Fourier peak amplitudes should thus be comparable to the amplitude of the single Fourier peak of a second-order grating (i.e. a grating such that $k_{\text{grating}} = k_{\text{in}}$), used successfully in the past to demonstrate high-performance surface emitting lasers [20, 21]. We can thus expect the threshold to be comparable for GAB lasers and surface emitting lasers, since the scattering losses are comparable.

3. Grating design and fabrication

It may seem uncertain at first whether single-mode operation, desired in each lasing wavelength region, would be preserved with GAB lasers, as the lasing mode corresponds to a high scattering order and thus to a relatively low-amplitude Fourier component. Furthermore, one could wonder if introducing disorder within the unit cell, for example by using a unit cell with a random sequence (the same random sequence being repeated to form the superlattice), would have a negative impact on the laser behavior, since it corresponds to more complex scattering paths. In order to verify these points, we fabricated lasers with relatively large unit cells and 'reduced' short-scale order. We chose a unit cell based on a Rudin–Shapiro (RS) aperiodic sequence. The RS sequence is notable because its Fourier spectrum is absolutely continuous, which makes it akin to purely random series. The RS sequence is a deterministic aperiodic sequence that can be generated in a two-letter alphabet by iteration of this inflation rule [22–25]: AA → AAAB, AB → AABA, BA → BBAB, BB → BBBA. In the case of gratings, this two-letter alphabet can be transcribed into a sequence of low- and high-refractive-index layers (e.g. A for low index, B for high index). A 2D RS array was used in [26] to demonstrate laser action in a pseudo-random medium.

We designed a grating for operation on five distinct wavelengths. The unit cell is composed of 108 quarter-wave layers in a sequence given by the sixth-generation RS sequence (128 elements) where we removed the last 20 elements. This truncation shortened the superperiod and increased accordingly the spacing between the Fourier peaks, so as to fit exactly five peaks within the gain spectrum of the laser. The unit cell is repeated 25 times to form the superlattice. The number of repetitions of the unit cell was chosen so that the total length of the grating is about 2.5 mm. The quarter-wave layers are defined with respect to a central wavelength $\lambda = 8.4\,\mu$m. The precise sequence of the unit cell is given here[7] and is also represented in figure 4(a).

Figures 4(b) and (c) show the Fourier transforms of, respectively, the unit cell and the full grating, together with a transfer-matrix (T-matrix) calculation of the reflection spectrum (red), computed using a commercial T-matrix code (Film Wizard), of a 1D dielectric stack of quarter-wavelength layers with refractive indices 3.16 and 3.18, arranged in the same sequence as the grating we designed. We estimated the effective index of the etched and non-etched layers using finite-element simulations (COMSOL Multiphysics). At the positions of high-amplitude Fourier components, we observe sharp peaks in reflectivity marking the opening of a bandgap.

[7] H = high index, L = low index; 25 repetitions of (HHHLHHLHHHHLLLHLHHHLHHLHLLLHHHLHH-HHLHHLHHHHLLLHLLLLHLLHLHHHLLLHLHHHLHHLHHHHLLLHLHHHLHHLHLLLHHHLHLLLH-LLHLLLLH).

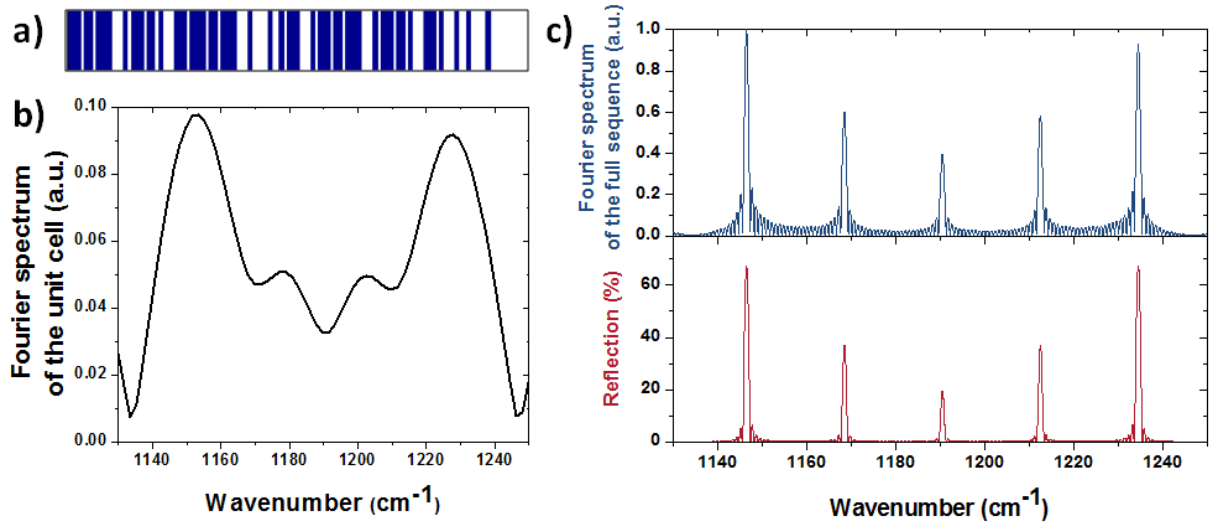

Figure 4. (a) Schematic diagram of the spatial refractive index profile of the unit cell. Blue bars represent low-index layers. (b) Fourier transform of the unit cell. (c) Fourier transform (blue) and reflection spectrum (red) computed with a transfer matrix code for a 1D stack of low (3.16) and high (3.18) index layers, for the full GAB sequence consisting of 25 repetitions of the unit cell shown in (a). The x-axis for the Fourier spectra are scaled by 2 to take into account the fact that lasing occurs at wavelengths such that $1/\lambda = k_{\text{grating}}/2$, where k_{grating} are the wavenumbers of the Fourier spectra peaks.

The amplitude of the five Fourier peaks was designed to compensate for the finite linewidth of the gain, in order to obtain a flat net gain. In other words, we compensated for the higher gain experienced by the central wavelength by reducing the amplitude of the corresponding Fourier component and thus the reflectivity.

The grating was fabricated as a buried grating on bound-to-continuum QCLs designed for operation at $\lambda = 8.4\,\mu$m. The QCL wafer used in this work was grown by Metalorganic chemical vapor deposition (MOCVD) on conducting InP:S substrate [27]. The lower cladding structure consists of a thick InP layer (InP:Si, $n = 1 \times 10^{17}\text{cm}^{-1}$, $d = 3.5\,\mu$m), a grading layer (InGaAsP:Si, $n = 1 \times 10^{17}\text{cm}^{-1}$, $d = 300$ Å) and an InGaAs layer (InGaAs:Si, $n = 3 \times 10^{16}\text{cm}^{-1}$, $d = 5200$ Å). The active region grown on top of the lower cladding is similar in design to the one described in [28]. It is composed of 35 repetitions of the following sequence: **13**/47/**12**/52/**11**/53/**9**/17/**44**/25/**36**/27/**32**/27/**25**/28/**21**/31/**18**/34/**16**/39/**15**/42, where the AlInAs barriers are in boldface and the n-doped ($4.9 \times 10^{16}\text{cm}^{-1}$) layers are underlined. The thicknesses are given in angstroms. The upper cladding grown on the active region is symmetric to the lower cladding with respect to the active region. The structure is finally capped with a highly doped InP layer (InP:Si, $n = 5 \times 10^{18}\,\text{cm}^{-1}$, $d = 0.5\,\mu$m). Electroluminescence from very-low-quality-factor (practically no feedback) mesa structures was measured, with a peak at 1190 cm^{-1} and a full-width at half-maximum of about 250 cm^{-1}. We used these values to adjust the design of the gratings.

Fabrication of the buried gratings is initiated by the removal of the upper cladding down to the 520 nm thick InGaAs layer by wet etching in a HCl:H_2O (1:1) solution. Electron beam lithography and reactive ion etching to a depth of 300 nm were then used to define the gratings

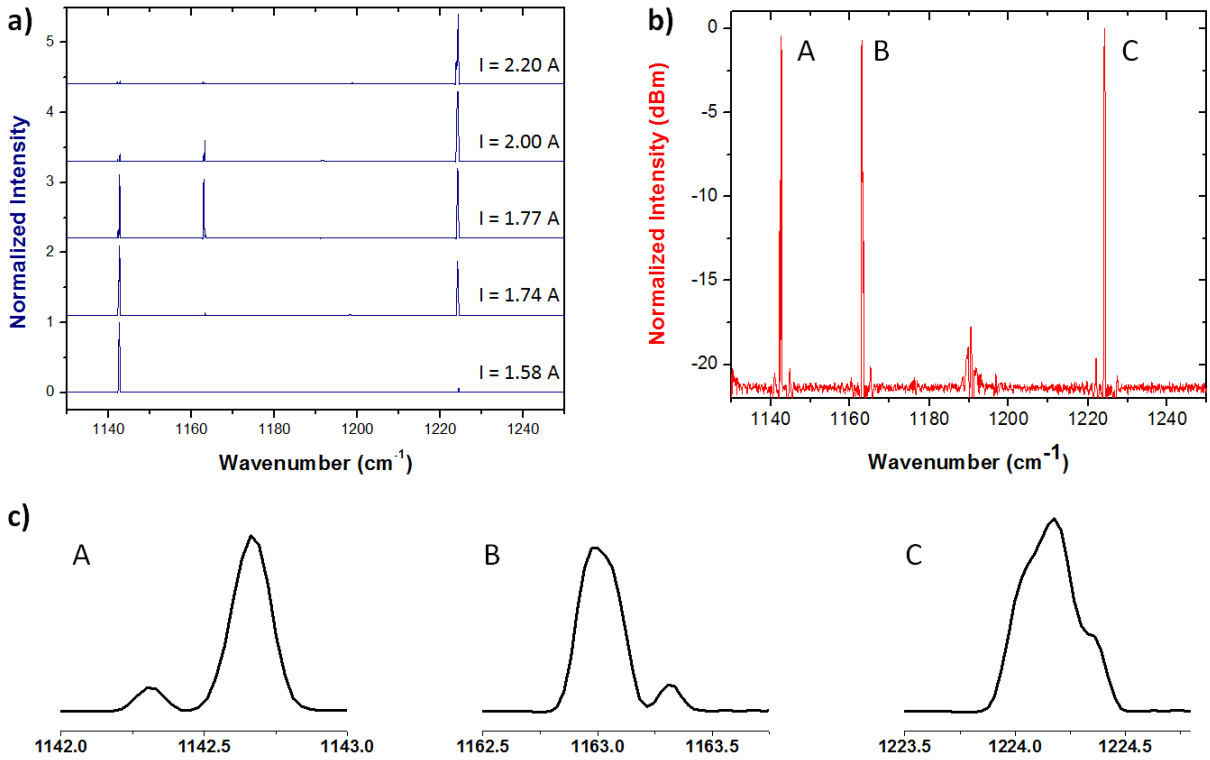

Figure 5. Experimental results for the five-wavelength grating design. (a) Lasing spectrum of a typical device with AR coating, 2.5 mm long and 23 μm wide, operated at room temperature in pulsed mode, with a repetition rate of 20 kHz and a pulse length of 100 ns, at different currents. (b) Log-scale plot of the central spectrum represented in panel (a) ($I = 1.77$ A). (c) Zoom-in spectra of peaks A, B and C referenced in panel (b), on a linear scale.

into the InGaAs layer. The same upper cladding as the original one was then regrown on the structure to bury the grating. Laser ridges 20, 23 and 26 μm wide were subsequently defined using reactive ion etching. Electrical passivation was achieved by depositing 450 nm of SiN using plasma-enhanced chemical vapor deposition. Top and bottom metallization consisted of Ti (15 nm)/Au (450 nm). The fabricated devices were cleaved to $\simeq$2.5 mm length, indium mounted on copper heat sinks and characterized in pulsed operation, with a pulse length of 100 ns and a repetition rate of 20 kHz.

In order to eliminate Fabry–Perot longitudinal modes, we deposited on the front facet of the lasers an anti-reflection (AR) coating composed of a bilayer of YF_3 and ZnSe [6]. After deposition, lasing was suppressed for Fabry–Perot lasers processed on the same chip as the devices with gratings.

4. Experimental results

The laser spectra at different biases of a typical device with a five-wavelength grating are presented in figure 5(a). The spectra feature up to three simultaneous lasing peaks at room temperature. A blue-shift of the gain with increasing bias results in the suppression of the

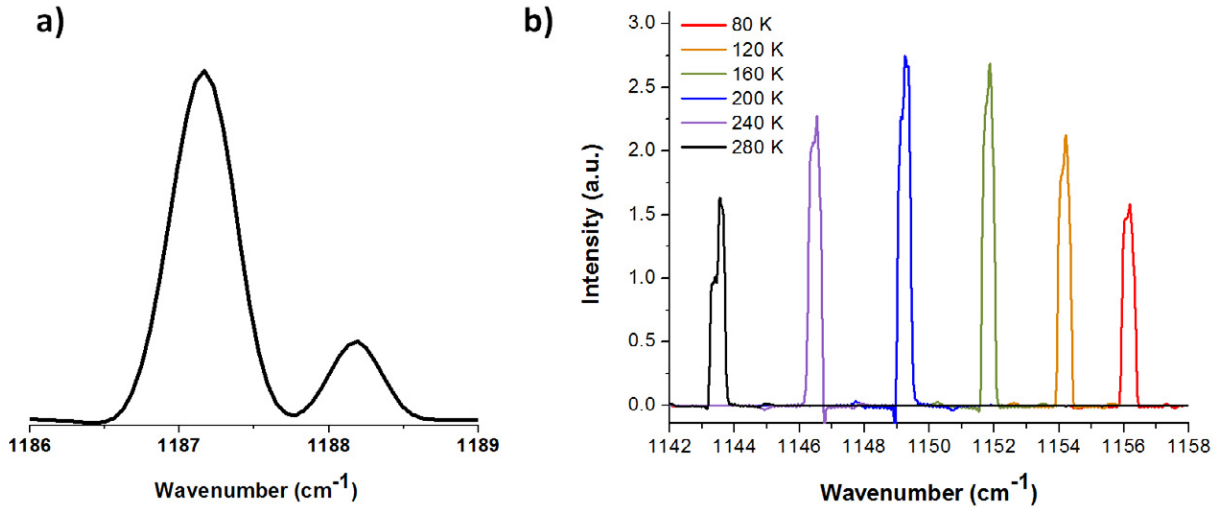

Figure 6. (a) Lasing spectrum of a DFB laser processed on the same chip as the GAB gratings studied here, operated in similar conditions. (b) Zoom-in of peak A in figure 5(b) at different temperatures, from 80 to 280 K.

reddest peaks and the apparition of a third peak on the blue side for a large bias (see figure 5(a)). We observe that the position of the lasing peaks is systematically red-shifted by about 0.5% compared to the calculated reflection peaks. This error can be attributed to our imperfect knowledge of the effective refractive indices of the layers. As explained above, the relative amplitude of the Fourier components of this grating was designed to compensate for the gain lineshape in order to obtain a flatter net gain. The fact that two of the central wavelengths never lase indicates that we underestimated the gain linewidth in our calculations and overly favored the extremum wavelengths.

So far, we have left aside the question of why multi-mode lasing can be expected at all in QCLs. If the grating does provide five narrow regions with higher net gain, that does not necessarily mean that lasing has to occur in all five regions. In contrast, basic laser theory suggests that once a first mode starts lasing, gain should be clamped, which in turn prevents any further mode to reach the lasing threshold. Multi-mode operation is possible in QCLs, because of their low threshold for spatial hole burning (SHB) instability [29]. This instability comes into play when the gain recovery time becomes comparable to or smaller than the carrier diffusion time, so that the gain grating created by the lasing mode longitudinal pattern is not washed out but persists, leaving regions of the waveguide where gain is available for other modes to start lasing. It is thus because of SHB that our devices feature several lasing modes. However, further study beyond the scope of this paper would be needed to quantify the role of the SHB instability in multi-wavelength QCLs and the impact of an AR coating on its threshold.

Figure 5(b) shows a log-scale plot of the central spectrum in figure 5(a), on which a side-mode suppression ratio (SMSR) of 20 dB is obtained for the three lasing modes. A central island of Fabry–Perot modes is observed, indicating a residual reflectivity of the AR coating and a relatively high net gain region stemming from the two other Fourier peaks that were expected to select two other single-mode wavelengths.

A closer look at each peak reveals that they are not rigorously single-mode (see figure 5(c)). Peaks A and B are doublets corresponding to the two band edges of the band gap. Measuring

the spacing between the two band-edge modes enables us to estimate the coupling coefficient κ, as it is a measure of the bandgap width. Following [30], we use $\kappa = \pi n_{\mathrm{av}} \cdot \Delta(k_{\mathrm{gap}}) \simeq 5\,\mathrm{cm}^{-1}$, where $n_{\mathrm{av}} \simeq 3.17$ is the average effective index in the laser waveguide and $\Delta(k_{\mathrm{gap}}) \simeq 0.5\,\mathrm{cm}^{-1}$ (cf figure 5(c)). In comparison, we measured the coupling coefficient for DFB lasers fabricated on the same chip (figure 6(a)). We obtain $\Delta(k_{\mathrm{gap}}) \simeq 1\,\mathrm{cm}^{-1}$, which corresponds to $\kappa \simeq 10\,\mathrm{cm}^{-1}$. As expected, the coupling coefficient for GABs is lower than that for DFB lasers, but this is not an issue for QCLs as they are usually processed into long waveguides (typically 2–3 mm long). Peak C is composed of three peaks. The third peak probably corresponds to a higher-order lateral mode, as the lasers were processed in relatively wide ridges (23 μm wide).

We verified the temperature tuning performance of the GAB lasers by monitoring the position of peak A in figure 5(b) at regular temperature intervals from 80 K up to room temperature. The results are shown in figure 6(b). A continuous temperature tuning of $0.06\,\mathrm{cm}^{-1}\,\mathrm{K}^{-1}$ is obtained. This is comparable to typical values obtained for QCLs operating in the long-wavelength infrared range [31].

5. Conclusion

In summary, we introduced GABs as a generalization of several existing approaches to design gratings having multiple selected spatial frequencies. The use of aperiodic sequences opens a range of new possibilities for the Fourier spectrum engineering of superstructure gratings. We used such gratings to provide distributed feedback and demonstrate simultaneous multi-wavelength lasing of mid-infrared QCLs on up to three wavelengths, each having an SMSR of 20 dB. More generally, the concept of GABs could find significant applications wherever multi-band reflectors are needed.

Acknowledgments

We thank M A Kats, P Genevet and N Yu for helpful discussions. We acknowledge support from the Air Force Office of Scientific Research (MURI 67N-1069926) and the Harvard Nanoscale Science and Engineering Center. This work was carried out in part at the Center for Nanoscale Systems at Harvard University—a member of the National Nanotechnology Infrastructure Network, which is supported by the National Science Foundation (NSF). LDN acknowledges support from the Air Force program 'Deterministic Aperiodic Structures for On-chip Nanophotonic and Nanoplasmonic Device Applications' under award no. FA9550-10-1-0019 and from NSF Career Award no. ECCS-0846651. RD acknowledges support of the Steve W Chaddick Endowed Chair of OptoElectronics at Georgia Tech.

References

[1] Lyakh A, Maulini R, Tsekoun A, Go R, Von der Porten S, Pflügl C, Diehl L, Capasso F and Patel K 2010 High-performance continuous-wave room temperature 4.0-μm quantum cascade lasers with single-facet optical emission exceeding 2 W *Proc. Natl Acad. Sci. USA* **107** 18799

[2] Gmachl C, Sivco D, Colombelli R, Capasso F and Cho A Y 2002 Ultra-broadband semiconductor laser *Nature* **415** 883

[3] Faist J, Beck M, Aellen T and Gini E 2001 Quantum-cascade lasers based on a bound-to-continuum transition *Appl. Phys. Lett.* **78** 147

[4] Fujita K, Edamura T, Furuta S and Yamanishi M 2010 High-performance, homogeneous broad-gain quantum cascade lasers based on dual-upper-state design *Appl. Phys. Lett.* **96** 241107
[5] Yao Y, Wang X, Fan J-Y and Gmachl C 2010 High performance 'continuum-to-continuum' quantum cascade lasers with a broad gain bandwidth of over 400 cm^{-1} *Appl. Phys. Lett.* **97** 081115
[6] Hugi A, Terazzi R, Bonetti Y, Wittmann A, Fischer M, Beck M, Faist J and Gini E 2009 External cavity quantum cascade laser tunable from 7.6 to 11.4 μm *Appl. Phys. Lett.* **95** 061103
[7] Lee B G, Kansky J, Goyal A K, Pflügl C, Diehl L, Belkin M A, Sanchez A and Capasso F 2009 Beam combining of quantum cascade laser arrays *Opt. Express* **17** 16216
[8] Sigrist M W 1994 *Air Monitoring by Spectroscopic Techniques* (New York: Wiley)
[9] Colley C, Hebden J, Delpy J, Cambrey A, Brown R, Zibik E, Ng W, Wilson L and Cockburn J 2007 Mid-infrared optical coherence tomography *Rev. Sci. Instrum.* **78** 123108
[10] Belkin M A, Capasso F, Belyanin A, Sivco D, Cho A Y, Oakley D, Vineis C and Turner G 2007 Terahertz quantum-cascade-laser source based on intracavity difference-frequency generation *Nat. Photon.* **1** 288
[11] Kogelnik H and Shank C V 1972 Coupled-wave theory of distributed feedback lasers *J. Appl. Phys.* **43** 2327
[12] Straub A, Gmachl C, Sivco D L, Sergent A M, Capasso F and Cho A Y 2002 Simultaneously at two wavelengths (5.0 and 7.5 μm) singlemode and tunable quantum cascade distributed feedback lasers *Electron. Lett.* **38** 565
[13] Jayaraman V, Chuang Z-M and Coldren L 1993 Theory, design, and performance of extended tuning range semiconductor lasers with sampled gratings *IEEE J. Quantum Electron.* **29** 1824
[14] Ashcroft N W and Mermin N D 1976 *Solid State Physics* (New York: Holt, Rinehart and Winston)
[15] Tohmori Y, Yoshikuni Y, Ishii H, Kano F, Tamamura T, Kondo Y and Yamamoto M 1993 Broad-range wavelength-tunable superstructure grating (SSG) DBR lasers *IEEE J. Quantum Electron.* **29** 1817
[16] Schroeder M R 2010 *Number Theory in Science and Communication* (Berlin: Springer)
[17] Avrutsky I, Ellis D, Tager A, Anis H and Xu J 1998 Design of widely tunable semiconductor lasers and the concept of binary superimposed gratings (BSG's) *IEEE J. Quantum Electron.* **34** 729
[18] Mahler L, Tredicucci A, Beltram F, Walther C, Faist J, Beere H E, Ritchie D A and Wiersma D 2010 Quasi-periodic distributed feedback laser *Nat. Photonics* **4** 165
[19] Macía E 2008 *Aperiodic Structures in Condensed Matter: Fundamentals and Applications* (London: Taylor and Francis)
[20] Hofstetter D, Faist J, Beck M and Oesterle U 1999 Surface-emitting 10.1 μm quantum-cascade distributed feedback lasers *Appl. Phys. Lett.* **75** 3769
[21] Pflügl C, Austerer M, Schrenk W, Golka S, Strasser G, Green R P, Wilson L R, Cockburn J W, Krysa A B and Roberts J S 2005 Single-mode surface-emitting quantum-cascade lasers *Appl. Phys. Lett.* **86** 211102
[22] Dal Negro L and Boriskina S V 2011 Deterministic aperiodic nanostructures for photonics and plasmonics applications *Laser Photonics Rev.* at press
[23] Dulea M, Johansson M and Riklund R 1992 Localization of electrons and electromagnetic waves in a deterministic aperiodic system *Phys. Rev.* B **45** 105
[24] Kroon L, Lennholm E and Riklund R 2002 Localization-delocalization in aperiodic systems *Phys. Rev.* B **66** 094204
[25] Gopinath A, Boriskina S, Reinhard B and Dal Negro L 2008 Deterministic aperiodic arrays of metal nanoparticles for surface-enhanced Raman scattering (SERS) *Nano Lett.* **8** 2423
[26] Yang J-K, Boriskina S V, Noh H, Rooks M J, Solomon G S, Dal Negro L and Cao H 2010 Demonstration of laser action in a pseudorandom medium *Appl. Phys. Lett.* **97** 223101
[27] Huang Y, Ryou J H, Dupuis R, Pflügl C, Capasso F, Sun K, Fischer A and Ponce F 2011 Optimization of growth conditions for InGaAs/InAlAs/InP quantum cascade lasers by metalorganic chemical vapor deposition *J. Cryst. Growth* **316** 75

[28] Wittmann A, Gresch T, Gini E, Hvozdara L, Hoyler N, Giovannini M and Faist J 2008 High-performance bound-to-continuum quantum-cascade lasers for broad-gain applications *IEEE J. Quantum Electron.* **44** 36

[29] Gordon A *et al* 2008 Multimode regimes in quantum cascade lasers: from coherent instabilities to spatial hole burning *Phys. Rev.* A **77** 053804

[30] Morthier G and Vankwinkelberge P 1997 *Handbook of Distributed Feedback Laser Diodes* (Boston, MA: Artech House)

[31] Green R P *et al* 2004 High-performance distributed feedback quantum cascade lasers grown by metalorganic vapor phase epitaxy *Appl. Phys. Lett.* **85** 5529